Control of frequency chirp in nanosecond-pulsed laser spectroscopy. 1. Optical-heterodyne chirp analysis techniques

Richard T. White, Yabai He, and Brian J. Orr

Centre for Lasers and Applications, Macquarie University, Sydney, NSW 2109, Australia

Mitsuhiko Kono and K. G. H. Baldwin

Research School of Physical Sciences and Engineering, Australian National University, Canberra, ACT 0200, Australia

Received January 6, 2004; revised manuscript received March 29, 2004; accepted April 5, 2004

We evaluate ways to analyze optical-heterodyne measurements of frequency chirp in pulsed, single-longitudinal-mode output from lasers (or other coherent light sources) that operate on nanosecond time scales. The instantaneous frequency is extracted from the beat signal generated between a continuous-wave reference beam and the output of the pulsed source. Three analysis techniques are tested: Fourier-transform, direct curve fitting, and electronic mixing. We use synthetic beat waveforms based on actual experimental parameters to evaluate the three methods and apply these chirp-measurement techniques to an injection-seeded optical parametric oscillator system. © 2004 Optical Society of America

OCIS codes: 040.2840, 120.5050, 190.4970, 230.4320, 300.6320.

1. INTRODUCTION

When pulsed lasers (or other coherent light sources) are used for precision spectroscopy, it is important to know how the optical phase and amplitude evolve during the light pulse. Optical-heterodyne (OH) techniques can provide such information for nanosecond pulses of coherent, single-longitudinal-mode (SLM) light. In this approach, light from a continuous-wave (cw) reference source is combined at a photodetector (PD) with light from the pulsed SLM source.[1–12] One can analyze the resultant beat waveform to determine the evolution of the optical phase and thereby derive the instantaneous-frequency profile of the SLM light pulse. The beat signal is centered about the difference frequency between the two light fields at the PD, so that a bandpass filter at that frequency can be used to remove unwanted frequency components that are well separated from it. A large difference frequency (typically several hundred megahertz) is chosen to generate a large number of beat oscillations during the optical pulse and to ensure that the Fourier components of the beats and of the coherent SLM pulse are widely separated. It also takes advantage of the lower noise levels that usually occur at high frequencies.

For an injection-seeded pulsed system, such as a pulse-amplifier chain[1–10] or an optical parametric oscillator (OPO),[11,12] the source of cw seed radiation may also serve as the reference source. It is then necessary to displace the cw frequency actively, for example, by using an acousto-optic modulator (AOM) operating at the desired difference frequency. This provides the reference beam, as depicted in Fig. 1 and considered subsequently in this paper.

It is customary to analyze the beat waveform by means of Fourier-transform (FT) techniques.[13,14] In this paper we evaluate two additional ways to analyze the beat signal, and we compare their results with those of the FT approach. One method directly extracts time-dependent phase-perturbation information in the (otherwise) sinusoidal modulation waveform by a least-squares fitting procedure. The other technique employs a matched pair of electronic mixers; the modulation and beat frequencies are introduced into the mixer inputs, and the intermodulation output yields the quadrature phase information needed to reconstruct both the instantaneous frequency profile and the intensity profile.

In this paper we evaluate the performance of the three methods, using a synthetic intensity profile for an optical pulse based on the measured parameters of a pulsed SLM coherent light source. The three techniques are also applied simultaneously to the actual pulsed SLM signal output of an injection-seeded OPO that is based on periodically poled $KTiOPO_4$ (PPKTP) pumped by a custom-built frequency-doubled Nd:YAG laser with a relatively long pulse duration (~27 ns). Detailed characterization of the frequency chirp from this PPKTP OPO system is demonstrated in the following paper.[12]

2. EXPERIMENT

As illustrated in Fig. 1, the output of the pulsed SLM coherent light source to be characterized is combined collinearly with the output of a narrowband, frequency-stable cw reference laser and focused onto a square-law PD to produce a beat waveform. If the cw frequency is sufficiently offset from the frequency of the pulsed coherent source, OH beats in the intensity profile of the optical

0740-3224/2004/091577-09$15.00

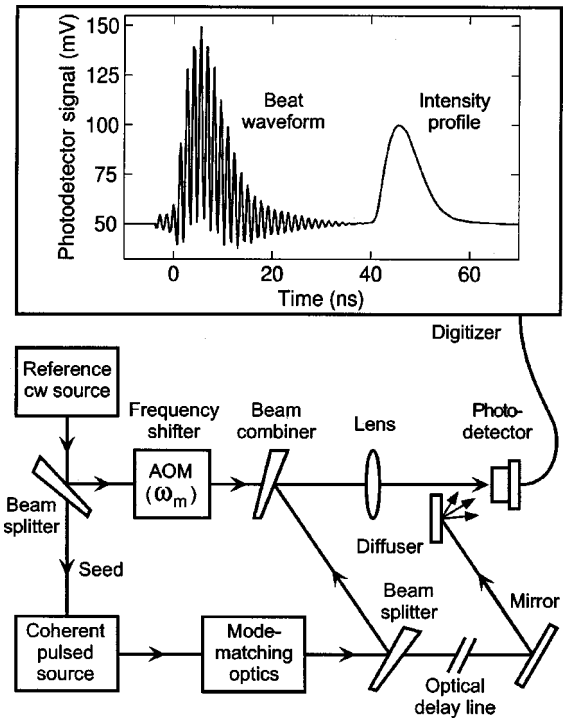

Fig. 1. Schematic of the (OH) technique used to measure the optical phase evolution of pulses from a coherent light source. The AOM is driven at angular frequency ω_m. Inset, unchirped synthetic beat waveform and its optically delayed pulse intensity profile.

pulse can be observed at frequency f_{beats} (approximated by the AOM frequency for the system in Fig. 1), provided that their frequency is within the detection system's range of working frequencies f_{det}. For a Gaussian-shaped pulse with full width at half-maximum (FWHM) duration Δt, this condition reduces to

$$(0.44/\Delta t) < f_{\text{beats}} < f_{\text{det}}. \tag{1}$$

For a typical upper value of f_{det}, i.e., ~1 GHz, narrowband SLM optical pulses with durations longer than ~1 ns can be analyzed by the OH techniques described in this paper. In addition, the detection system must also have a sufficiently high sampling rate of at least twice the Nyquist critical frequency; if $f_{\text{det}} = 1\,\text{GHz}$, the minimum sampling rate required is therefore ~2 GSa s^{-1}, where Sa is one digital sample.

By virtue of its narrow bandwidth, low noise characteristics, and stable frequency, the cw seed source provides an ideal means of generating the frequency-shifted reference beam. Furthermore, because the wave-front direction of the generated pulse is determined primarily by the seed beam, an injection-seeded pulsed coherent source has minimal sensitivity to any apparent phase shift that may result from tilt variations between the cw reference and pulsed beams.[15]

In the simplest case, the cw and pulsed radiation fields (with electric vectors $\mathbf{E}_{\text{cw}}$ and $\mathbf{E}_p$, respectively) are assumed to be linearly polarized plane waves[2]:

$$\mathbf{E}_{\text{cw}}(t) = \mathbf{E}_{\text{cw}}{}^0 \exp[i(\omega_0 - \omega_m)t)] + \text{c.c.}, \tag{2}$$

$$\mathbf{E}_p(t) = \mathbf{E}_p{}^0(t)\exp[i\langle\omega\rangle t + i\phi(t)] + \text{c.c.}, \tag{3}$$

where ω_0 and ω_{m} are the angular frequencies of the cw radiation field and of the AOM, respectively, and c.c. denotes a complex conjugate. Any phase perturbations during the pulse evolution are assigned entirely to $\phi(t)$ because the central value $\langle\omega\rangle$ of the pulsed field's angular frequency is time independent. For example, for the FT method $\langle\omega\rangle$ may correspond to the peak of the pulsed power spectrum. However, in the present context, the absolute value of $\langle\omega\rangle$ is immaterial because we are concerned only with the beat frequency.

The instantaneous-frequency profile, $f_{\text{inst}}(t)$, of the pulse is then defined as[2]

$$f_{\text{inst}}(t) = (2\pi)^{-1}\text{d}\phi(t)/\text{d}t. \tag{4}$$

It should be noted that $f_{\text{inst}}(t)$ is relative to the central frequency ($\langle\omega\rangle/2\pi$) and is zero if there are no phase perturbations. The voltage signal generated by the PD has the form

$$V_{\text{PD}} \propto |\mathbf{E}_{\text{cw}}(t) + \mathbf{E}_p(t)|^2 = |\mathbf{E}_{\text{cw}}{}^0|^2 + |\mathbf{E}_p{}^0(t)|^2 + \mathbf{E}_{\text{cw}}{}^0\mathbf{E}_p{}^0(t)\{\exp[i(\langle\omega\rangle + \omega_m - \omega_0)t + i\phi(t)] + \text{c.c.}\}. \tag{5}$$

The first term in Eq. (5), which is due to the cw beam alone, can be neglected. The second term represents the intensity envelope of the optical pulse, and the third term is the OH interference term (comprising positive- and negative-frequency components). A modulation index, $\mu(t)$, can be included in the interference term to account for imperfect overlap of the two beams.[2] To evaluate the optical phase perturbations, one must isolate the third term and extract $\phi(t)$ from it.

Frequency chirp commonly refers to an approximately linear or monotonic change in $f_{\text{inst}}(t)$, which can include quadratic and other higher-order chirp terms. Because real pulses can exhibit complicated $f_{\text{inst}}(t)$ behavior, we have found it useful to define two parameters that measure the variation in $f_{\text{inst}}(t)$ during the pulse.[11] The utility of these two chirp parameters is demonstrated later in this paper and in Ref. 12. The first parameter, denoted Δf_{inst}, is simply the difference between the maximum and the minimum frequency excursions, such that

$$|\Delta f_{\text{inst}}| = (f_{\text{inst}})_{\text{max}} - (f_{\text{inst}})_{\text{min}}. \tag{6}$$

The sign of Δf_{inst}, which is taken to be negative if $(f_{\text{inst}})_{\text{max}}$ precedes $(f_{\text{inst}})_{\text{min}}$ and positive otherwise, indicates whether the chirp increases or decreases during the pulse. However, this sign is of limited value when $f_{\text{inst}}(t)$ fluctuates about a central value with no pronounced overall trend. The second measure of the variation in $f_{\text{inst}}(t)$ is the range of frequencies covered by a straight-line fit to the $f_{\text{inst}}(t)$ profile (the linear-fit definition). We have employed both definitions of the variation in $f_{\text{inst}}(t)$ in our seeded OPO experiments (which exhibit predominantly linear chirp) with comparable results.[11,12]

The choice of the time period over which Δf_{inst} and the linear fit are defined is arbitrary, but the interval between the 10%-intensity points of the pulse profile is consistent with previous reports.[1,2,11] In many applications, such as nonlinear-optical wavelength conversion, only the central part of the pulse with the highest peak powers is signifi-

cant. In this case, Δf_{inst} measured between the 50%-intensity points is likely to be a more useful quantity.

We test the performance of the chirp analysis techniques by using computer-generated waveforms that are based on a measured intensity profile (~8-ns FWHM, ~14-ns 10%-intensity interval) from a pulsed PPKTP OPO,[11] smoothed to reduce the noise level. The OPO pulse was measured by a 1-GHz Si P–I–N photodiode (New Focus 1601; 0.4-ns rise time) and a 2-GHz digitizing oscilloscope (Tektronix TDS794D) with a sampling rate of 4 GSa s^{-1}, matching that of our detection system.

The synthetic PD waveform (Fig. 1, inset) is generated by forming numerical beats between the synthetic pulse and a frequency-shifted (−730-MHz) cw reference beam. The optically delayed pulse ~40 ns later permits pulse-envelope subtraction for each pulse rather than pulse averaging,[9] although this procedure has no significant benefit at high beat frequencies (e.g., >700 MHz, as in this study). In the inset the pulse is unchirped and has a constant modulation index (μ) of 0.5,[2] included to simulate incomplete overlap of the two beams consistent with previous experimental observations.[1,2,11]

In the next three sections we evaluate the performance of the three analysis techniques, using synthetic pulses with various rates of linear chirp. This evaluation is also valid for quadratic and higher-order chirp because, on sufficiently small time scales, a given $f_{\text{inst}}(t)$ profile can be approximated by a sequence of linear chirps of varying slope.

3. FOURIER-TRANSFORM METHOD

We have employed a technique, similar to that devised by Fee *et al.*,[1] that entails Fourier transforming the beat signal. This FT technique has been used to characterize the optical phase properties of cw dye and Ti:sapphire lasers amplified in dye media[1–10] and, more recently, of an injection-seeded PPKTP OPO.[11] Figure 2 shows how Fourier transformation of a synthetic beat waveform yields a power spectrum that can then be filtered with a bandpass filter (three types of filter are shown) to select the positive-frequency interference term, which is explicit in the final part of relation (5). This filtered frequency-domain power spectrum is then backtransformed to the time domain. The magnitude and the angle of the resultant complex-valued data yield the amplitude and the phase, respectively, of the original optical pulse. The $f_{\text{inst}}(t)$ profile is then obtained from the optical phase by use of Eq. (4).

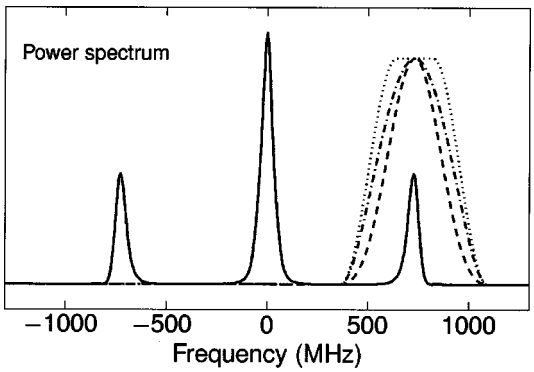

Fig. 2. Power spectrum of the beat waveform in Fig. 1 (solid curve) and the three filter functions superimposed: Blackman (dashed curve), first-order Blackman (dashed–dotted curve), and Tukey (r = 0.75; dotted curve).

A key to the accuracy of the FT algorithm is its ability to isolate the positive interference term in relation (5) while it retains all its phase and amplitude information. It is important to minimize the overlap between the interference terms and the dc-centered frequency component [which is due to the pulse profile, $|\mathbf{E}_p{}^0(t)|^2$, and to the cw level, $|\mathbf{E}_{\text{cw}}{}^0|^2$]. Slight overlap of the two components was found to be the largest source of error in previous measurements.[2,4] To minimize overlap it is useful to employ a relatively large beat frequency or to reduce the dc-centered component by subtracting the delayed intensity profile from the beat signal. In previous reports of cw lasers that were pulse amplified in dye media,[1–10] adequate separation was attained with a beat frequency of as much as 400 MHz. In our preliminary PPKTP OPO research[11] we further reduced the overlap by using an AOM frequency of ~730 MHz, although this required a larger detection-system bandwidth (3-dB rolloff at ~1 GHz) and sampling rate (4 GSa s^{-1}).

The choice of frequency-domain filter is also important. A rectangular filter centered at the peak beat frequency and with a width equal to the peak beat frequency provides optimal isolation of the interference term while giving zero attenuation across its passband. However, such a filter allows significant spectral leakage to occur because of its sharp edges, complicating interpretation in the time domain. There is a trade-off between the flatness of the filter and the sidelobe level of its Fourier transform.[13] We have compared the performance of three filters of varying flatness: Blackman, first-order Blackman (as defined in Ref. 4), and Tukey.[13] It should be noted that, in data-windowing applications, such filters are usually applied in the time domain.

Each of the three filter functions shown in Fig. 2 is defined in terms of a parameter δ that corresponds to the zero-to-zero width relative to the peak beat frequency. The Tukey filter is specified by a second parameter, r, defining the combined width of its two tapered regions normalized to δ; the filter then evolves from rectangular to Hanning type as r varies from 0 to 1.

The FT algorithm was applied to an unchirped synthetic beat waveform, with several values of δ for each filter, so any deviation of $f_{\text{inst}}(t)$ from a constant value is an artifact of the FT algorithm. For values of δ greater than ~1, modulation appears on the portion of the $f_{\text{inst}}(t)$ curve that corresponds to the rising edge of the pulse. This modulation occurs because the filter extends into the dc-centered component of the frequency spectrum, the highest-frequency components of which correspond to the rising edge of the pulse. The optimum value of δ (δ_{opt}) is chosen to be the largest value for which these modulations are no longer significant (i.e., less than 1 MHz in this study). The results, for unchirped 8- and 25-ns (FWHM) pulses, are listed in Table 1. These results indicate how the three filters are likely to perform for actual chirped pulses.

Table 1. Characteristics of the Filter Functions Used for Chirp Analysis by the FT Method[a]

Filter Type	δ_{opt} ~8-ns Pulse	δ_{opt} ~25-ns Pulse	Filter Width (FWHM $\times\delta$)
Blackman	1.1	1.5	0.406
First-order Blackman[b]	0.9	1.3	0.541
Tukey			
$r = 0$ (rectangle)	0.6	0.9	1.0
$r = 0.25$	0.7	1.1	0.875
$r = 0.5$	0.7	1.2	0.75
$r = 0.75$	0.8	1.2	0.625
$r = 1$ (Hanning)	1	1.3	0.5

[a] Indicative results are shown for both short (8-ns FWHM; Ref. 11) and long (25-ns FWHM; Ref. 12) unchirped synthetic pulses.
[b] As defined in Ref. 4.

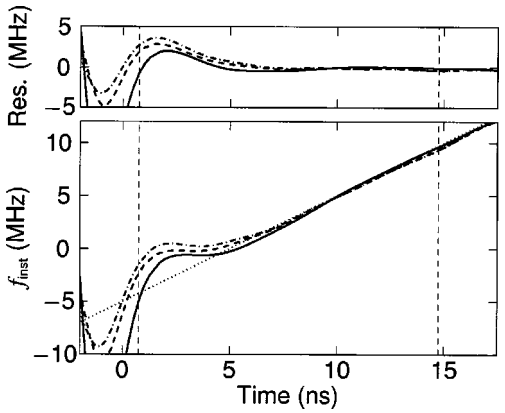

Fig. 3. FT algorithm applied to the synthetic 8-ns pulse with a linear chirp rate of +1 MHz ns^{-1}. Bottom, calculated $f_{inst}(t)$. Top, residual deviation of $f_{inst}(t)$ from the input chirp profile. Results are shown for three filter functions: Tukey (solid curve; $r = 0.75$, $\delta = 0.8$), first-order Blackman (dashed curve; $\delta = 0.9$), and Blackman (dashed–dotted curve; $\delta = 1.1$). The dotted line (bottom) is the input chirp profile, and the vertical dashed lines define the 10%-intensity interval for the input pulse.

Figure 3 shows the $f_{inst}(t)$ curves generated by the FT algorithm when it is applied to the synthetic 8-ns pulse with a linear frequency chirp of +1 MHz ns^{-1}. The largest residual excursion is due to the fast-rising edge of the synthetic pulse. To investigate this effect, we removed the high-frequency components by applying a low-pass filter to the intensity profile, which reduced this residual excursion to <1 MHz. Alternatively, by using the output intensity profile as an input pulse, as described in Ref. 9, we achieved a similar reduction. Note that for a purely Gaussian synthetic pulse the residual excursion is $\ll$0.1 MHz.

The optimized filters were then applied to synthetic pulses with various total chirp values, and the resultant calculated chirp was compared to the input chirp value. The percent chirp deviations plotted in Fig. 4 show that the Blackman and the first-order Blackman filters are less accurate than the Tukey filter with $r = 0.75$, which reproduces the synthetic linearly chirped $f_{inst}(t)$ profiles to within ~10% uncertainty across a broad chirp range. This Tukey filter is therefore preferred because it yields smaller relative errors than the other two forms of filter.

4. DIRECT-FIT METHOD

Our second chirp-analysis technique models the beat waveform directly by using a least-squares fitting procedure. This direct-fit approach provides a clear picture of how the instantaneous frequency $f_{inst}(t)$ varies during a single OPO pulse without transferring to the frequency domain.

The phase and frequency information of the OPO pulse is contained in the third (cross) term of relation (5), which is a product of electric field amplitudes and a sinusoidal phase term. We can extract the first two terms (cw and pulsed intensity profiles) as well as the electric field amplitude of the cross term from the recorded beat waveform. It therefore remains to determine the sinusoidal phase term. This we do by using a least-squares fit to a polynomial for the phase, thereby separating the sinusoidal phase term from intensity and amplitude terms such that the phase term can be analyzed directly over the pulse duration.

The direct-fit procedure reconstructs the intensity terms of the beat waveform, as in relation (5), by application of Savitzky–Golay moving-window (SGMW) smoothing[14] to the recorded beat waveform to remove the oscillating cross term. One then retrieves the cross term by subtracting the reconstructed intensity terms from the recorded beat waveform, with its amplitude obtained by SGMW smoothing of the absolute value of the cross term and multiplication by $\pi/2$. The phase term, extracted by

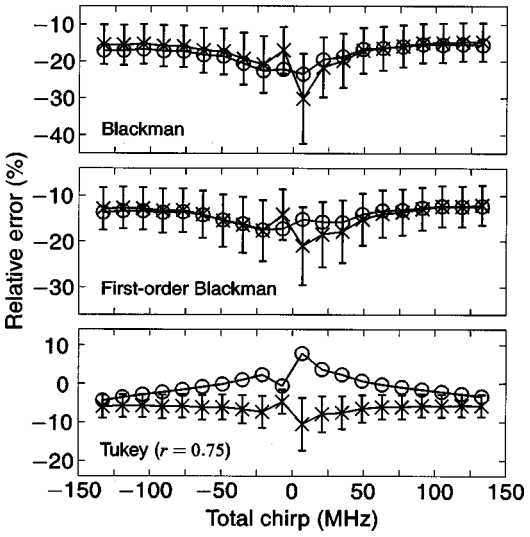

Fig. 4. Percent error in the output of the FT algorithm normalized to the input chirp applied to a range of synthetic pulses (8-ns FWHM duration) with linear chirp rates that range from −10 to +10 MHz ns^{-1}. The error is plotted against the total chirp within the 10%-intensity window (14 ns). Circles and crosses, Δf_{inst} and linear-fit definitions of the chirp, respectively. Results are shown for Blackman, first-order Blackman, and Tukey ($r = 0.75$) filter functions, with the filter's width parameter δ set at δ_{opt}. The error bars in the linear-fit data show the percent of standard deviation of the linear fit from the $f_{inst}(t)$ curve compared with the total chirp, within the 10%-intensity interval.

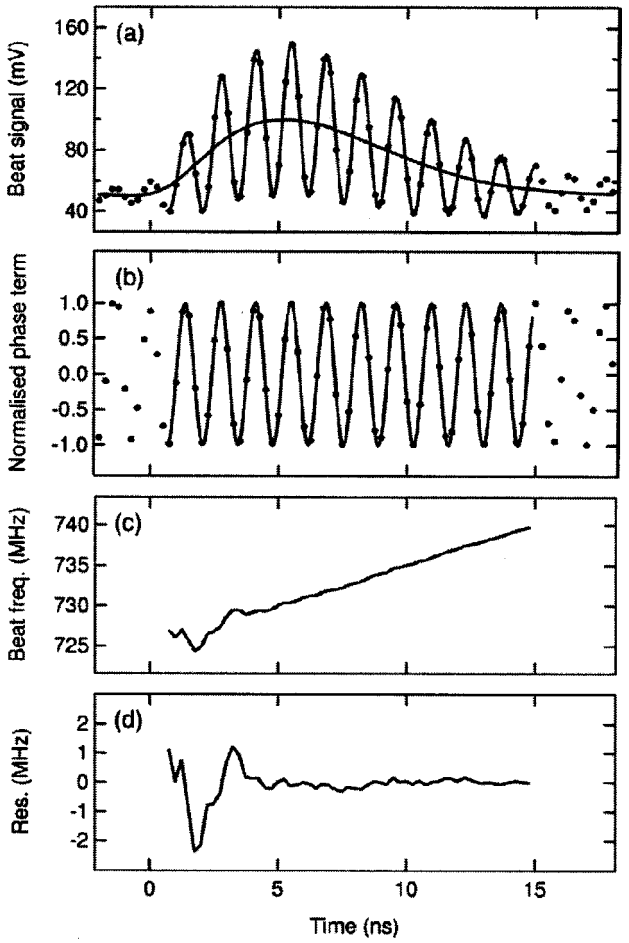

Fig. 5. Direct-fit method applied to the synthetic 8-ns pulse with a linear chirp rate of $+1$ MHz ns^{-1}. (a) Input beat-waveform data points (dots) and model fit within the 10%-intensity interval, plus reconstructed intensity profile. (b) Normalized phase term (dots) and least-squares fit with polynomial phase, within the 10%-intensity interval (solid curve). (c) Calculated beat frequency for a moving window that is ~2 oscillation periods wide. (d) Residual deviation of $f_{\text{inst}}(t)$ from the input chirp profile.

division of the cross term by its reconstructed amplitude, is represented by a least-squares fit of the form $[a + b \sin(c_0 + c_1 t + c_2 t^2 + \ldots)]$, where the first two parameters, a and b, have nominal values of 0 and 1, respectively. The instantaneous frequency and model beat waveform are then derived from the fitted phase term parameters by use of Eq. (4) and relation (5).

This procedure is illustrated in Fig. 5, where it is shown applied to a synthetic 8-ns pulse with a linear frequency chirp of $+1$ MHz ns^{-1}. We used a total of 11 data points (~2 oscillation periods) and a third-order polynomial for SGMW smoothing[14] and applied it four times successively. In Fig. 5(a) the input beat waveform is represented by the 4-GSa s^{-1} sampled data points (dots) connected by a model beat-waveform fit within the 10%-intensity points of the input pulse; the smooth solid curve is the reconstructed intensity profile. The normalized phase term (dots) and its least-squares fit to a sinusoid with polynomial phase (solid curve) are shown in Fig. 5(b) over the 10%-intensity interval. The extracted instantaneous beat frequency, obtained by a moving window (~2 oscillation periods wide) and a second-order polynomial for the phase, and its deviation from the input instantaneous frequency are shown in Figs. 5(c) and 5(d), respectively.

The least-squares fit of the phase term is applied in two different ways. First, we can fit the phase of the whole section of interest by using a polynomial function of adjustable order (a second-order polynomial represents a linearly chirped frequency). We increase the order of the polynomial successively to determine the best fit. The second method uses a separate moving-window approach. For each data point we choose an adjustable number of surrounding data points to form a narrow region of the curve, fit this narrow region to the model function, and use the resultant fit only for this data point. We repeat the fit for all data points by shifting the moving window. This approach is useful, as it reveals phase perturbations over a narrow range.

It might appear that the amplitude of the cross term is proportional to the square root of the pulse intensity. However, this is a reasonable assumption only for small frequency chirp. For larger chirp, a broadband component (e.g., comprising several longitudinal modes) may gain intensity toward the end of the pulse at the cost of a reduction in the narrowband SLM component. The square root of the pulse intensity contains both narrowband and broadband contributions, whereas the amplitude of the cross term arises only from the narrowband component. Such a comparison offers a practical way to determine whether a broadband component exists in the pulsed output signal.

We verified the performance of this direct-fit method by applying the method to synthesized beat waveforms for different chirp rates, as for the FT method described in Section 3. The results, related to the linear-fit definition of chirp, are shown in Fig. 6. The corresponding Δf_{inst} chirp definition is not used here: It is identical to the linear-fit definition for a single direct fit of the entire beat waveform; it differs only slightly from the linear-fit definition if a moving-window direct fit is applied. The largest residual excursion is due to the fast-rising edge of the synthetic pulse, as shown in Fig. 5(d). We attribute this effect to a minor imperfection in reconstructing the inten-

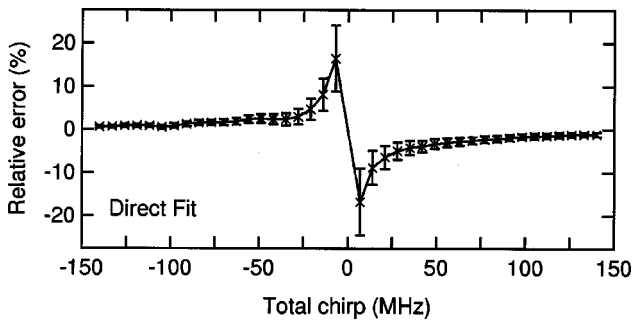

Fig. 6. Percent error in the output of the direct-fit algorithm applied to a range of synthetic pulses (8-ns FWHM duration) with linear chirp rates that range from -10 to $+10$ MHz ns^{-1}. The error is plotted against the total chirp within the 10%-intensity window (14 ns). Crosses, linear-fit definition only; error bars, percent of standard deviation (~0.5 MHz) of moving-window linear fits (over ~ 2 oscillation periods) from the input chirp profiles compared with the total chirp.

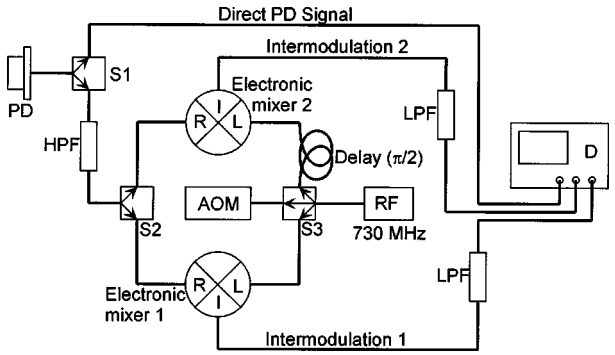

Fig. 7. Schematic of electronic mixing: PD, photodetector; RF, rf driver for the AOM; R, L, I, rf signal input, local oscillator (AOM) input, and intermodulation output of electronic mixers, respectively; D, digitizing oscilloscope; HPF, high-pass filter; LPF, low-pass filter; S1, S2, rf power splitters.

sity terms of the beat waveform at the fast-rising edge of the synthetic pulse. The overall agreement of the extracted instantaneous frequency is accurate and reliable. In contrast to those of the FT method (Section 3) and the electronic mixer method (Section 5 below), the residual excursion profiles of the direct-fit method are not affected significantly by the chirp rate and remain below ~2 MHz at all chirp rates. Thus we are able to correct actual experimental measurements by using the known residual error profile of the synthetic beat waveform based on the actual pulse-intensity profile.

5. ELECTRONIC MIXER METHOD

Both of the methods described above require a high-frequency data-acquisition system (at least 4 GSa s^{-1} for a 730-MHz modulation) and, as has been shown, can be subject to errors that arise from the choice of filter to suppress unwanted frequencies or from truncation of the fitting polynomial. A third pulse chirp-analysis technique employs electronic rf mixing technology[16] and requires only readily available data-acquisition systems with modest bandwidths (several hundred megahertz).

Feeding the rf signal driving the AOM along with the PD output into an electronic mixer demodulates the beat signal to yield only the frequency-chirp components (typically <100 MHz). The demodulated output is equivalent to that which would have been obtained from an OH beat signal by use of the original (unshifted) seed laser but with the advantage that low-frequency detector noise has been removed.

Figure 7 shows the circuit diagram used for the mixer technique. The beat-waveform signal produced by the PD is separated into two equal channels by a rf power splitter (S1; Mini-Circuits ZFSC-3-1). The direct PD signal channel is recorded by a 5-GSa s^{-1}, 0.5-GHz digitizing oscilloscope (Tektronix TDS3054). The other channel is sent to a simple high-pass filter (Mini-Circuits BHP-300; −30-dB insertion loss at 180 MHz) to remove the dc offset ($|\mathbf{E}_{cw}{}^0|^2$) in relation (5) and other low-frequency components [e.g., $|\mathbf{E}_p{}^0(t)|^2$]. The filtered signal is further separated equally into two channels by a second rf power splitter (S2; Mini-Circuits ZFSC-3-1). These two channels are then introduced into the respective reference input ports of two electronic mixers (Mini-Circuits ZAD-2).

The 730-MHz rf wave produced by the AOM driver (Brimrose Model VFF-100-300-V) is separated into three channels in the ratio 8:1:1 by a third rf power splitter (S3; homemade). The highest-power channel is used to drive the AOM; the other two channels provide the reference frequency for the local input ports of the electronic mixers. The output product signal channels from the two electronic mixers are recorded by the digitizer as intermodulation signals. One of the two local oscillator signals from splitter S3 is delayed via a short (~50-mm) passive delay line. The length of the delay line is adjusted to ensure that the phase difference between the two intermodulation waveforms is close to $\pi/2$. The intermodulation waveform data are obtained by use of the low-bandpass (150-MHz) mode on the digitizer to reduce high-frequency cross talk from the rf driver at ~730 MHz.

A rf electronic mixer generates an intermodulation product voltage $V_I \propto V_R V_L$ from two rf voltages, the local oscillator voltage (V_L) and the rf input voltage (V_R). In the present case, $V_R = V_{PD}$, and V_L is obtained from the rf output of the AOM. When V_I is observed through a low-pass filter, the high-frequency terms in V_I (near ω_m and $2\omega_m$) are eliminated. We can also create another intermodulation output whose phase is shifted by $-\pi/2$ from the initial phase by introducing a delay line from the local oscillator. Therefore we have, for the two quadratures,

$$V_I{}^S = C^S \mu(t) |\mathbf{E}_p{}^0(t)| \sin[\phi(t) + (\omega_0 - \langle\omega\rangle)t], \quad (7)$$

$$V_I{}^C = C^C \mu(t) |\mathbf{E}_p{}^0(t)| \cos[\phi(t) + (\omega_0 - \langle\omega\rangle)t], \quad (8)$$

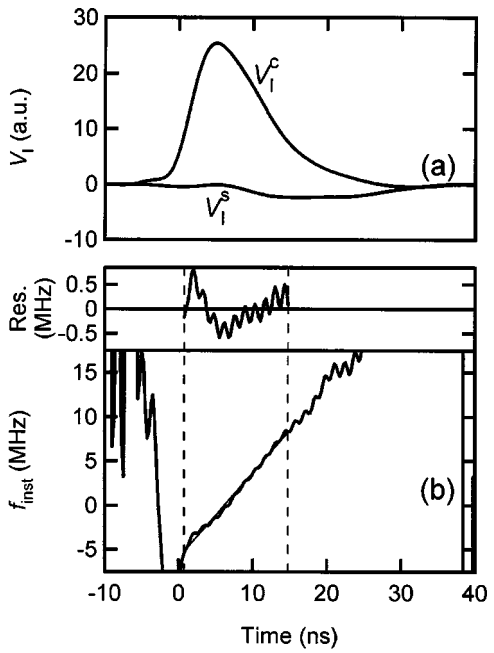

Fig. 8. Mixer simulation applied to the synthetic 8-ns pulse (linear chirp rate, +1 MHz ns^{-1}). (a) Simulated intermodulation quadrature outputs $V_I{}^S$ and $V_I{}^C$. (b) Bottom, calculated $f_{inst}(t)$; top, residual frequency difference from a linear fit to $f_{inst}(t)$. The frequency of the local oscillator input is 730 MHz. Vertical dashed lines define the 10%-intensity interval.

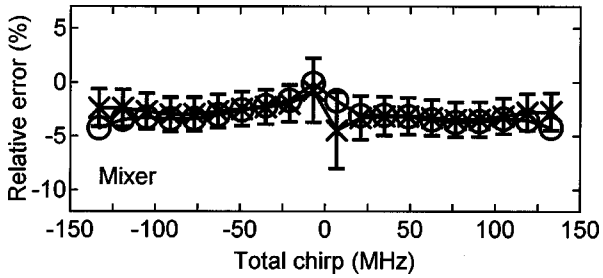

Fig. 9. Percent error in the output of the mixer method applied to a range of synthetic pulses (8-ns FWHM duration) with linear chirp rates that range from -10 to $+10$ MHz ns^{-1}. Crosses, linear fit; circles, Δf_{inst}. Error bars show the percent of standard deviation of the residuals between the linear fit and the calculated $f_{\text{inst}}(t)$ values compared with the total chirp. The frequency of the local oscillator input was 730 MHz.

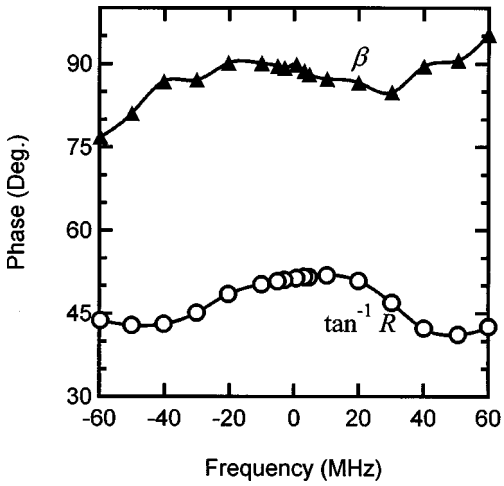

Fig. 10. Mixer dispersion data showing phase delay β (triangles) and the arctangent of amplitude ratio R (circles) as functions of intermodulation frequency (centered at ~730 MHz).

where $\mu(t)$ is the modulation index[2] that was introduced in the context of relation (5). The instrument-dependent factors C^S and C^C are proportional to $|\mathbf{E}_{\text{cw}}{}^0|$; they are exactly equal if the two mixer channels are perfectly balanced. The initial phase of V_L is assumed to be zero. Temporal profiles for the instantaneous frequency, $f_{\text{inst}}(t)$, and the pulse, $|\mathbf{E}_p{}^0(t)|^2$, can then be obtained by use of $V_I{}^S$ and $V_I{}^C$ as the imaginary and the real components, respectively.

Figure 8 shows the mixer simulation results, obtained with a synthetic OH beat signal input with a $+1$-MHz ns^{-1} chirp and a 730-MHz synthetic local oscillator input. The predicted $\pi/2$ phase-shifted mixer outputs from the two channels are shown in Fig. 8(a). In this simulation a low-pass filter was applied with an attenuation profile given by $[1 + (f/f_c)^{2n_f}]^{-1/2}$, where f is the frequency at which attenuation occurs, f_c is the cutoff frequency (-3-dB power), and n_f is the number of filter elements. Values of $f_c = 150$ MHz and $n_f = 6$ were used to simulate the experimentally observed attenuation at 730 MHz.

The lower portion of Fig. 8(b) shows the calculated evolution of $f_{\text{inst}}(t)$, with residual frequency differences from a straight-line least-squares fit shown above it. Within the 10%-intensity interval this fit has a slope (0.964 ± 0.011 MHz ns^{-1}) that is within 4% of the original synthetic chirp. The corresponding residual frequency differences are less than 0.85 MHz, and the standard deviation of the residuals, which indicates the degree of scatter, is 0.33 MHz. The relative percentage error for both chirp definitions is shown in Fig. 9 as a function of the total input chirp during the (14-ns) 10%-intensity interval. The mixer method yields chirp values that are consistently lower than the input chirp but within 5% of the input chirp value.

6. PRACTICAL MIXER CONSIDERATIONS

We have so far considered the relative merits of the three chirp-analysis techniques when they are used in a simulated measurement of synthetic pulses. In practice, the mixer technique introduces additional experimental uncertainties that are not present in the other techniques. For example, the phase shift between the two electronic mixers might not be exactly $\pi/2$, and the amplitudes of the two mixer signals might not be equal. We therefore redefine the actual mixer output as $V_I{}^{C\prime}$ and $V_I{}^{S\prime}$, respectively, so that

$$V_I{}^C = (RV_I{}^{C\prime} - V_I{}^{S\prime}\cos\beta)/\sin\beta, \tag{9}$$

$$V_I{}^S = V_I{}^{S\prime}, \tag{10}$$

where R and β are an amplitude ratio and a phase difference, respectively. These parameters can be obtained by a least-squares fit of the reconstructed temporal profile to the original temporal profile, $|\mathbf{E}_p{}^0(t)|^2$. The dispersion thus described includes the effects of all the electronic components that follow the photodiode.

We have measured the dispersion of the mixer system over a ± 60-MHz range of frequency shifts from the reference frequency by replacing the PD output to the mixer input with another variable-frequency rf driver. The frequency dependence of phase delay β and the arctangent of amplitude ratio R are shown in Fig. 10. As can be seen, β varies by less than 10°, whereas a similar fractional variation occurs because of the change in R.

To test the effect of β and R on the accuracy of the results, we processed the synthetic mixer output shown in Fig. 8(a) ($+1$-MHz ns^{-1} chirp) by taking account of the system's measured dispersion characteristics (Fig. 10). The resultant reconstructed temporal profile is almost indistinguishable from the undispersed calculation (residual differences range from $+0.4$ to -1.0%), whereas the residual difference from the synthetic temporal profile ranges from $+4$ to -6%. The standard deviation of the dispersion-processed $f_{\text{inst}}(t)$ profile from the input frequency profile is 0.4 MHz; it differs from the undispersed processed signal by a standard deviation of only 0.1 MHz, indicating that dispersion effects are negligible for this synthetic pulse.

Finally, the electronic mixers in practice exhibit harmonic distortion (i.e., they do not produce exact trigonometric functions) in their intermodulation outputs, even when monochromatic cw inputs are used; this distortion causes variation in the output $f_{\text{inst}}(t)$ value. Measurements of this $f_{\text{inst}}(t)$ variation have been performed by use

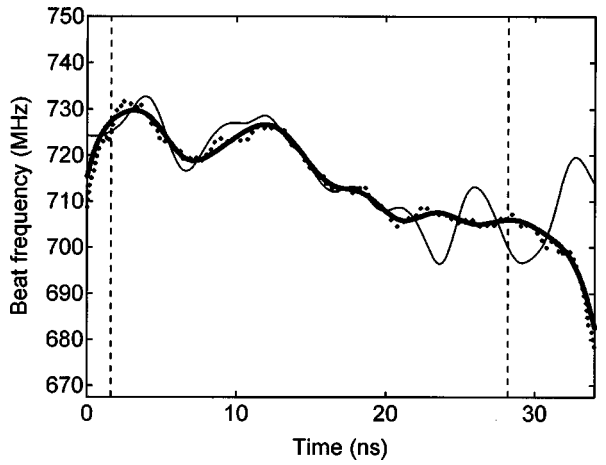

Fig. 11. Instantaneous beat-frequency evolution for output from a pulsed PPKTP OPO, shown over the 10%-intensity interval for the FT (heavier solid curve), direct-fit (dotted curve), and mixer (finer solid curve) methods. Vertical dashed lines define the 50%-intensity interval.

of unchirped cw rf inputs of adjustable frequency. The results show only small variations that range from <1 MHz at the reference frequency to <3 MHz at ±60 MHz offset to the reference frequency.

7. EXPERIMENTAL BENCHMARKING

To compare these techniques experimentally, we simultaneously applied all three chirp-analysis methods to the OPO system described in Ref. 12 for which relatively long (~27-ns) pump pulses are employed. Using an arrangement similar to that shown in Fig. 7, we split the PD signal to provide a raw beat signal to one input channel of a TDS3054 digitizing oscilloscope and applied the other signal to the inputs of two electronic mixers. The mixer reference channels were fed by the ~730-MHz rf signal driving the AOM. Some low-level rf cross talk was consequently observed between the mixer ports. The OPO was operated at just over twice the unseeded threshold pump power at a wavelength of 841.70 nm, slightly detuned from the free-running center wavelength of 841.82 nm, to provide a measurable chirp.[11,12]

The chirp evolution calculated by the three techniques is shown in Fig. 11. Agreement within the 10%-intensity interval defined by the figure margins is very good, and it is significantly better within the 50%-intensity interval, particularly for the FT and direct-fit methods, the results for which are almost indistinguishable. The larger frequency excursions for the mixer method may arise from cross talk between the mixer ports or the digitizer channels or from the dispersion effects discussed in Section 6. Within the 10% or 50% intensity limits, the respective standard deviations between the FT and direct-fit methods are 1.4 or 1.0 MHz; the corresponding standard deviations between the FT and mixer methods are 7.5 or 3.6 MHz. These deviations are considerably less than the FT-limited optical bandwidth (~17.5 MHz FWHM) for the temporal profile (~25 ns FWHM) of this OPO pulse.[12]

8. CONCLUSIONS

We have evaluated three ways to analyze beat waveforms obtained by OH measurement of SLM output from pulsed coherent light sources on nanosecond time scales. All three methods are applicable for accurate determination of the frequency chirp that arises from optical phase perturbations, and all can be implemented in real time for pulses with repetition rates of several tens of hertz.

A comparison of the results presented in Figs. 4, 6, and 9 shows that all three techniques yield similar chirp results that are within 10% of the synthetic input chirp value. The residual deviations in the direct-fit results are insensitive to variation of the chirp rate and amount to no more than ~2 MHz (at the rising edge of the pulse). With the FT method and the preferred Tukey filter, the Δf_{inst} deviation is of the order of a few percent over much of the total chirp range, apart from the (submegahertz) deviations at low chirp. Depending on the chirp-measurement criteria (linear fit or Δf_{inst}) and the type of filtering used, the methods can yield percentage chirp deviations that are slightly above or below the synthetic pulse value. However, even for extremely large chirps that exceed 100 MHz, the deviation from the synthetic chirp value is much less than 10 MHz. For smaller total chirp values of ~10 MHz, which are more typical of our PPKTP OPO experiments,[11,12] the deviation is small (<2 MHz), particularly compared with the FT-limited optical bandwidth (55 MHz FWHM) for the temporal profile (~8 ns FWHM) of the synthetic pulse.

The mixer technique should in principle yield the same result as the FT and direct-fit methods. However, in its practical implementation the filtering, dispersion, and amplitude characteristics can influence the accuracy of the measurement, although the synthetic pulse analysis shows that their influence has only a small effect on the uncertainty of the final result. Although the mixer method does not yield quite so accurate chirp measurements as the other techniques in the OPO experiment, it has the practical advantage that it can be implemented with only a few simple electronic components. Moreover, it does not need a fast digitization system (with a bandwidth at least several times the AOM frequency, i.e., several gigahertz). In practice, the mixer output can be recorded with a detection-system bandwidth that exceeds only the maximum beat-frequency excursion from the mixer reference frequency (i.e., several hundred megahertz).

We have applied these techniques to an injection-seeded PPKTP OPO system pumped by a frequency-doubled SLM Nd:YAG laser with a relatively long pulse duration (~27 ns). All three methods yield similar results for the instantaneous frequency profile $f_{\mathrm{inst}}(t)$. In the following paper,[12] we report in more detail on the chirp characteristics of this OPO system.

ACKNOWLEDGMENTS

We acknowledge financial support from the Australian Research Council.

B. J. Orr's e-mail address is brian.orr@mq.edu.au.

REFERENCES

1. M. S. Fee, K. Danzmann, and S. Chu, "Optical heterodyne measurement of pulsed lasers: toward high-precision pulsed spectroscopy," Phys. Rev. A **45**, 4911–4924 (1992).
2. S. Gangopadhyay, N. Melikechi, and E. E. Eyler, "Optical phase perturbations in nanosecond pulsed amplification and second-harmonic generation," J. Opt. Soc. Am. B **11**, 231–241 (1994).
3. N. Melikechi, S. Gangopadhyay, and E. E. Eyler, "Phase dynamics in nanosecond pulsed dye laser amplification," J. Opt. Soc. Am. B **11**, 2402–2411 (1994).
4. S. Gangopadhyay, "Optical phase distortions in nanosecond laser pulses and their effects on high resolution spectroscopy," Ph.D. dissertation (University of Delaware, Dover, Del., 1995).
5. K. S. E. Eikema, W. Ubachs, W. Vassen, and W. Hogervorst, "Precision measurements in helium at 58 nm: ground state Lamb shift and the $1\,^1S-2\,^1P$ transition isotope shift," Phys. Rev. Lett. **76**, 1216–1219 (1996).
6. K. S. E. Eikema, W. Ubachs, W. Vassen, and W. Hogervorst, "Lamb shift measurement in the $1\,^1S$ ground state of helium," Phys. Rev. A **55**, 1866–1884 (1996).
7. I. Reinhard, M. Gabrysch, B. Fischer von Weikersthal, K. Jungmann, and G. zu Pulitz, "Measurement and compensation of frequency chirping in pulsed dye laser amplifiers," Appl. Phys. B: Lasers Opt. **63**, 467–472 (1996).
8. S. D. Bergeson, A. Balakrishnan, K. G. H. Baldwin, T. B. Lucatorto, J. P. Marangos, T. J. McIlrath, T. R. O'Brian, S. L. Rolston, C. J. Sansonetti, J. Wen, N. Westbrook, C. H. Cheng, and E. E. Eyler, "Measurement of the He ground state Lamb shift via the two-photon $1\,^1S-2\,^1S$ transition," Phys. Rev. Lett. **80**, 3475–3478 (1998).
9. S. D. Bergeson, A. Balakrishnan, K. G. H. Baldwin, T. B. Lucatorto, J. P. Marangos, T. J. McIlrath, T. R. O'Brian, S. L. Rolston, C. J. Sansonetti, J. Wen, C. H. Cheng, and E. E. Eyler, "Precision spectroscopy in He as a test of QED," Phys. Scr. **T83**, 76–82 (1999).
10. S. D. Bergeson, K. G. H. Baldwin, T. B. Lucatorto, T. J. McIlrath, C. H. Cheng, and E. E. Eyler, "Doppler-free two-photon spectroscopy in the vacuum ultraviolet: helium $1\,^1S-2\,^1S$ transition," J. Opt. Soc. Am. B **17**, 1599–1606 (2000).
11. R. T. White, Y. He, B. J. Orr, M. Kono, and K. G. H. Baldwin, "Pulsed injection-seeded optical parametric oscillator with low frequency chirp for high-resolution spectroscopy," Opt. Lett. **28**, 1248–1250 (2003).
12. R. T. White, Y. He, B. J. Orr, M. Kono, and K. G. H. Baldwin, "Control of frequency chirp in nanosecond-pulsed laser spectroscopy. 2. A long-pulse optical parametric oscillator for narrow optical bandwidth," J. Opt. Soc. Am. B **21**, 1586–1594 (2004).
13. F. J. Harris, "On the use of windows for harmonic analysis with the discrete Fourier transform," Proc. IEEE **66**, 51–83 (1978).
14. W. H. Press, S. A. Teukolsky, W. T. Vetterling, and B. P. Flannery, *Numerical Recipes in* FORTRAN 77: *The Art of Scientific Computing*, 2nd ed. (Cambridge U. Press, Cambridge, 1992).
15. A. V. Smith and M. S. Bowers, "Phase distortions in sum- and difference-frequency mixing in crystals," J. Opt. Soc. Am. B **12**, 49–57 (1995).
16. Watkins-Johnson Company, *RF and Microwave Designer's Handbook* (Watkins-Johnson Company, Palo Alto, Calif., 1993), p. 758.